AIP Advances

Interface state density distribution near conduction band edge at Al_2O_3/Mg-ion-implanted GaN interface formed after activation annealing using AlN cap layer

Cite as: AIP Advances **12**, 125224 (2022); https://doi.org/10.1063/5.0117321
Submitted: 31 July 2022 • Accepted: 06 December 2022 • Published Online: 21 December 2022

Yuki Hatakeyama and Masamichi Akazawa

Interface state density distribution near conduction band edge at Al_2O_3/Mg-ion-implanted GaN interface formed after activation annealing using AlN cap layer

Cite as: AIP Advances 12, 125224 (2022); doi: 10.1063/5.0117321
Submitted: 31 July 2022 • Accepted: 6 December 2022 •
Published Online: 21 December 2022

View Online Export Citation CrossMark

Yuki Hatakeyama and Masamichi Akazawa[a)]

AFFILIATIONS

Research Center for Integrated Quantum Electronics, Hokkaido University, Sapporo 060-0813, Japan

[a)]Author to whom correspondence should be addressed: akazawa@rciqe.hokudai.ac.jp

ABSTRACT

An interface state density (D_{it}) distribution near the conduction band edge (E_C) at the Al_2O_3/Mg-ion-implanted GaN interface was measured after ion implantation, annealing with an AlN protective cap, and cap layer removal. Mg ions were implanted into n-GaN with a Si concentration of 6×10^{17} cm^{-3} at a maximum Mg concentration of 2×10^{17} cm^{-3}, resulting in the maintenance of the n-type conduction in GaN even after the activation of Mg dopants. Activation annealing was carried out at 1250 °C for 1 min using an AlN cap layer. The complete removal of the AlN cap layer was accomplished by wet etching, which was confirmed by x-ray photoelectron spectroscopy. The photoluminescence spectrum showed donor–acceptor-pair emission after annealing, indicating the activation of Mg acceptors. By applying the capacitance–voltage method to a completed metal–oxide–semiconductor diode, we derived a continuous distribution of relatively low D_{it} below 5×10^{12} cm^{-2} eV^{-1}, which increased monotonically toward E_C in the range from $E_C - 0.15$ to $E_C - 0.45$ eV. Compared with the D_{it} distribution of the as-implanted sample, the density of the discrete level at $E_C - 0.25$ eV generated by divacancies markedly decreased upon 1250 °C annealing.

I. INTRODUCTION

GaN has a wide bandgap (3.4 eV),[1] high breakdown field (3.3 MV/cm),[2] high electron mobility (1000 cm^2/V s),[1] high saturation electron velocity (2.6×10^7 cm/s),[3] and good thermal conductivity (2.1 W/cm °C).[1] Therefore, GaN is a promising material for fabricating highly efficient power electronic devices. In addition, the metal–oxide–semiconductor (MOS) structure formed on a GaN-on-GaN layer exhibits excellent properties.[4–7] Therefore, we can expect the realization of high-efficiency high-power MOS field-effect transistors (FETs) with the advantageous properties derived from GaN. To fabricate a MOSFET, ion implantation is a useful method for selective doping. However, this method is not fully established for GaN. In particular, Mg ion implantation for forming p-type GaN was difficult in the past. Recently, the successful fabrication of p-type GaN by Mg ion implantation has been achieved by many researchers. The key factor of this achievement is appropriate annealing at a high temperature. To the best of our knowledge, the first successful fabrication was achieved by specific rapid thermal annealing (RTA) under a nitrogen overpressure of 2 MPa with sequential pulse heating up to 1400 °C to activate Mg acceptors; this method was referred to as multicycle RTA and developed to become symmetric multicycle RTA.[8–11] The fabrication was also realized in an ordinary furnace in which annealing at a temperature higher than 1230 °C in atmospheric pressure nitrogen was found to activate the implanted Mg acceptors.[12–15] Furthermore, ultrahigh-pressure annealing (UHPA) in 1 GPa nitrogen has been performed at temperatures up to 1480 °C, resulting in a high Mg activation rate of 70%.[16] On the other hand, deep levels and defects generated by Mg ion implantation and subsequent annealing have been studied in detail by electrical measurements and positron annihilation spectroscopy (PAS).[17–25] Nevertheless, the interface states near

the conduction band edge (E_C) at the insulator/Mg-ion-implanted GaN interface after the annealing for Mg acceptor activation have not been investigated, although they might affect the performance of inversion-type n-channel MOSFETs. In particular, after Mg ion implantation before activation annealing, divacancy defects consisting of nitrogen vacancies (V_N) and gallium vacancies (V_{Ga}), i.e., $V_N V_{Ga}$, were mainly detected by PAS and found to generate gap states at E_C − 0.25 eV.[21] After Mg activation, however, the reduction in density of these states has not been confirmed. Since electrical detection of the gap states near E_C is difficult using p-GaN MOS diodes owing to the long time constant of the gap states for majority carriers and also the absence of minority carriers in wide-gap material, n-GaN MOS diodes should be used for the investigation.

In this work, we investigated the gap state density (D_T) distribution near E_C at insulator/Mg-ion-implanted GaN formed after high-temperature annealing for Mg acceptor activation, using n-type GaN with low-dose Mg ion implantation, to confirm the reduction in the density of the defects generated by the implantation and to assess the process-damage-related interface disorder. Here, the gap states include the interface states and near-surface bulk defect states. As an insulator layer, the Al_2O_3 layer formed by atomic layer deposition (ALD) was used because it has been reported that an excellent insulator/n-type GaN interface can be obtained with this layer.[4,5]

II. EXPERIMENTAL PROCEDURE

The MOS diode preparation sequence is illustrated in Fig. 1. An n-type GaN epitaxial layer with a Si donor concentration (N_D) of 6.0×10^{17} cm^{-3} and a thickness of 3 μm was grown by metal–organic vapor phase epitaxy (MOVPE) on a free-standing n$^+$-GaN (0001) substrate. Mg ions were implanted at an energy of 50 keV and a dose of 1.5×10^{12} cm^{-2} with the incident angle of 7° to the normal incidence. The maximum Mg concentration was calculated to be 2×10^{17} cm^{-3} at a depth of 50 nm on the basis of the "stopping and range of ions in matter (SRIM)" computer code. Thereafter, a 200-nm-thick AlN cap layer was deposited by the sputtering method onto the top surface, while the back surface was not coated because the N-face is highly thermally stable even at 1230 °C.[14] The annealing for Mg acceptor activation was performed at 1250 °C for 1 min in atmospheric pressure nitrogen flow. After annealing, the AlN cap layer was removed by wet etching using tetramethylammonium hydroxide (TMAH) at 80 °C for 2 h. Since this etching is reported not to etch the GaN (0001) surface markedly,[26] we expected that the damage to the GaN surface should not be severe as shown later. During this wet etching with TMAH, the back surface was not protected because this side is used only for a large-area (chip size: 7 × 7 mm^2) ohmic contact, which is not deteriorated by the etching of the thick n$^+$-GaN substrate. Next, the sample was treated with a solution of HF:H_2O = 1:1 prior to the formation of the 30-nm-thick Al_2O_3 layer by ALD at 300 °C using trimethylaluminum and H_2O. The MOS structure was completed by the metallization of the Ni/Au circular top electrode (diameter: 300 μm) and the Ti/Au back ohmic contact. Finally, post-metallization annealing (PMA) was carried out at 300 °C for 3 h in laboratory air to minimize the interface state density according to the previous reports[4,5] describing that the interface disorder at the Al_2O_3/GaN interface is reduced by PMA in laboratory air and in atmospheric pressure nitrogen flow. The completed MOS diode was examined by capacitance–voltage (C–V) measurements. The complete removal of the cap layer by wet etching with TMAH was confirmed by x-ray photoelectron spectroscopy (XPS) using an Al-Kα x-ray source (1486.6 eV). Before XPS, each sample was treated with HF:H_2O = 1:1 to reduce the surface oxide. Photoluminescence (PL) measurement of as-implanted and annealed samples was conducted at 10 K using a He–Cd laser source.

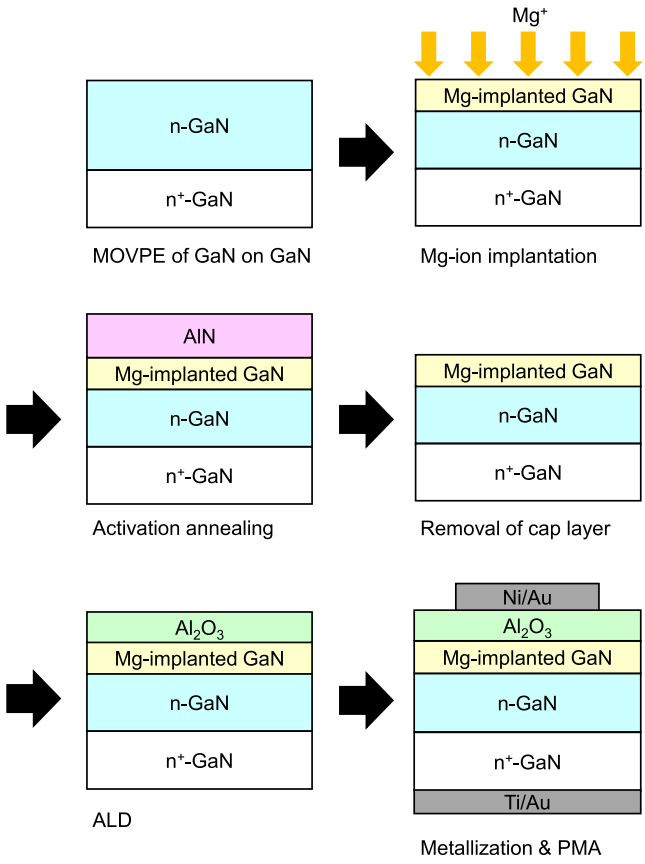

FIG. 1. Schematic diagram of sample fabrication sequence.

III. RESULTS AND DISCUSSION

The complete removal of the AlN cap layer after annealing was confirmed by XPS. Figure 2 shows the Al 2p spectra obtained after the etching of the AlN/GaN samples annealed at 1250 °C in comparison with that obtained for as-deposited thick AlN. Although etching at room temperature (RT) using a KOH solution was attempted, the Al 2p spectrum was detected even after etching for 72 h. By comparing the Al 2p spectra of the samples with 24 and 72 h KOH etching, we found that extending the etching time was not effective. Therefore, the annealed AlN was not completely removed by RT KOH etching. Presumably, the crystallization of the AlN layer upon annealing occurred to make this layer robust to RT

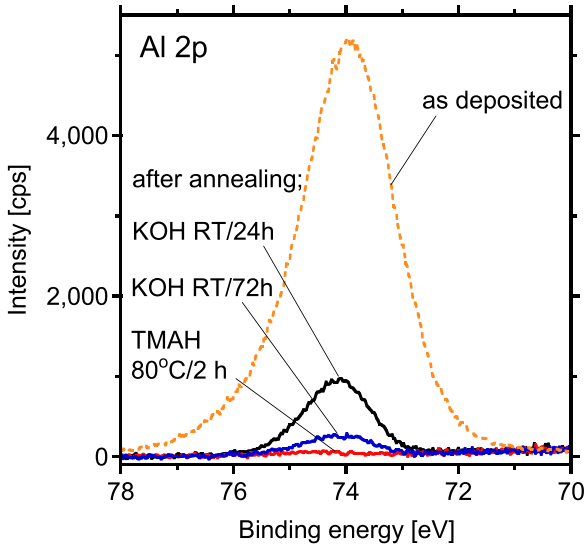

FIG. 2. XPS results for samples after various AlN cap layer removal processes performed subsequently to cap annealing.

KOH etching, especially near the interface. On the other hand, we found that etching with the TMAH solution at 80 °C for 2 h was effective in removing the AlN cap layer completely as shown in Fig. 2.

Figure 3 shows the Mg concentration [Mg] and Si concentration [Si] profiles measured by secondary ion mass spectroscopy (SIMS) for annealed GaN after implantation with the SRIM simulation results for [Mg] in the as-implanted GaN. The maximum [Mg] is well estimated by SIMS, although the channeling tail can be seen in the SIMS profile. The increases in [Mg] and [Si] toward the surface were due to surface contamination as usually seen in SIMS analysis. The maximum [Mg] was ~2 × 10^{17} cm^{-3} at around a depth of 40 nm. This concentration was well below [Si] of 6 × 10^{17} cm^{-3}, which indicates that the n-type conduction was maintained even after annealing, enabling the investigation of the interface states near E_C.

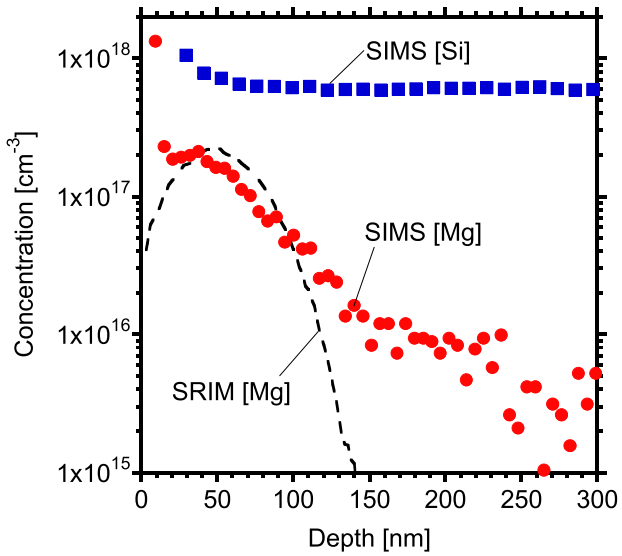

FIG. 3. [Mg] and [Si] profiles. Solid circles and rectangles show the SIMS [Mg] and SIMS [Si] profiles, respectively, for the Mg-implanted GaN after annealing at 1250 °C. (The AlN cap layer was removed before SIMS.) The broken line indicates the SRIM simulation result for the as-implanted GaN.

PL spectra of Mg-ion-implanted GaN obtained at 10 K before and after annealing with the AlN cap layer are plotted in Fig. 4. Upon annealing, emissions with distinct regular spacing (90 meV) at 3.27, 3.18, 3.09, 3.00, and 2.91 eV were observed. In previous reports,[27,28] these emissions have been attributed to donor–acceptor pair (DAP) emissions with phonon coupling. Therefore, these emission spectra indicated that the Mg acceptors were activated. However, the green luminescence (GL) at around 2.2 eV also became significant upon annealing, indicating that the defects generated by ion implantation still existed. This result is in good agreement with previous reports.[8,16,29,30] V_N-related defects are reported to be the origin of GL.[16,22,23,29] We will discuss on this later.

Figure 5(a) shows the C–V characteristics of the completed MOS diode with Mg-ion-implanted GaN after annealing. A small hysteresis and a distinct frequency dispersion can be seen, which indicates a non-negligible density of interface states near the conduction band edge. Even though the acceptor concentration (N_A) was well below N_D, the doping profile should have been nonuniform, especially near the surface, if the acceptors were activated. In Fig. 5(b), the $N_D - N_A$ profile derived from the 1 MHz C–V curve is plotted in the depth range corresponding to the surface Fermi level range where the interface states cannot respond to the bias sweep. In Fig. 5(b), the [Mg], [Si], and $N_D - N_A$ profiles expected for the 100% activation of Mg acceptors as a benchmark are also plotted. Here, to exclude the effect of the surface contamination in the SIMS [Si] profile, the expected profile was calculated by subtracting SIMS

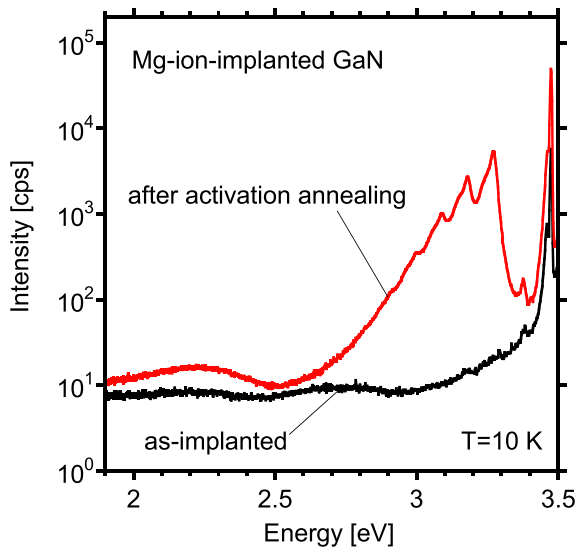

FIG. 4. PL spectra of Mg-implanted GaN before and after cap annealing at 1250 °C.

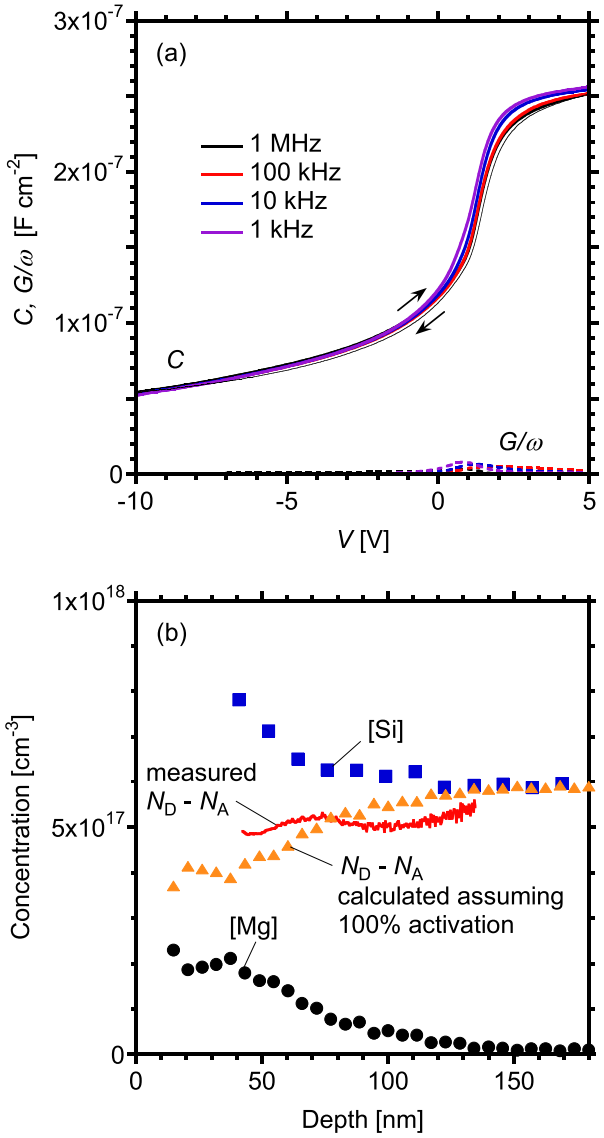

FIG. 5. (a) *C–V* characteristics of completed MOS diode. The thin black line indicates the *C–V* curve measured from the positive bias side to the negative bias side only for the 1 MHz curve to show the hysteresis, while the thick lines indicate the curve measured in the opposite direction. (b) $N_D - N_A$ profiles derived from 1 MHz *C–V* curve (solid line). The SIMS [Mg] (solid circles) and [Si] (solid rectangles) profiles in Fig. 3 appear again. The $N_D - N_A$ profile calculated for the 100% activation of Mg acceptors is also plotted (solid triangles).

[Mg] from 6.0×10^{17} cm^{-3}. In the depth range where the effect of the surface contamination is negligible, the accuracies are 1.5×10^{16} and 8×10^{15} cm^{-3} for [Si] and [Mg], respectively, while the accuracy of $N_D - N_A$ is 1×10^{16} cm^{-3}. Although the SIMS profile is affected by the surface contamination in the near-surface region, the maximum value of [Mg] is in good agreement with the SRIM simulation result as shown in Fig. 3. Empirically, the SIMS [Si] profile is severely affected by the surface contamination presumably because the molecule with the same mass number, e.g., CO, can be supplied easily from the atmosphere, while the [Mg] profile is less affected. Therefore, we believe that the effect of the surface contamination on [Mg] is significant only at small depths, and that [Mg] can be safely used for estimating the expected $N_D - N_A$ profile in the plot range in Fig. 5(b). The discrepancy between the measured and calculated $N_D - N_A$ profiles at a depth smaller than 80 nm can be explained by assuming a low activation rate. However, the deviation at a depth larger than 80 nm cannot be explained without assuming acceptor-like defects. The origin of this deviation will be discussed later.

Since the donor profile is not uniform, the application of the Terman method, which is frequently used because it is convenient to apply, is inappropriate for evaluating the D_{it} distribution. In this case, the high–low-frequency capacitance method might be useful.

Let us examine whether we can apply the high–low-frequency capacitance method to 1 MHz and 1 kHz *C–V* curves to derive the D_{it} distribution near E_C. In this method, D_{it} is derived from the high-frequency-limit capacitance C_{HF} and the low-frequency-limit capacitance C_{LF} according to[31]

$$D_{it} = \frac{1}{q^2}\left(\left(\frac{1}{C_{LF}} - \frac{1}{C_{OX}}\right)^{-1} - \left(\frac{1}{C_{HF}} - \frac{1}{C_{OX}}\right)^{-1}\right), \quad (1)$$

where C_{OX} is the oxide capacitance. Here, the position of the surface Fermi level E_{FS} corresponding to V was calculated by solving[31]

$$E_{FS} - E_C = \int_{V_0}^{V}\left(1 - \frac{C_{LF}}{C_{OX}}\right)dV, \quad (2)$$

where V_0 is the voltage for strong accumulation. The most important point in the application of this method is that 1 kHz and 1 MHz curves can be treated as low- and high-frequency limits, respectively. As the first approximation, the single-time-constant model can be applied to interface states, although the statistical distribution of time constants[28] should be considered rigidly. Namely, the time constant τ_{it} of an interface state for electrons is equal to the electron emission time constant of an electron trap[17,32,33] and is given by

$$\tau_{it} = \frac{1}{\sigma_n v_{th} N_C}\exp\left(\frac{E_C - E_{it}}{kT}\right), \quad (3)$$

where σ_n is the capture cross section of the interface state for electrons, v_{th} is the thermal velocity of electrons, N_C is the effective density of states at E_C, E_{it} is the energy for the interface state, k is the Boltzmann constant, and T is the temperature. Examples of calculation results of $f_{it} = 1/\tau_{it}$ as a function of E_{it} for different σ_n values are shown in Fig. 6. Although the energy dependence of σ_n has been measured for the insulator/Si interface,[34] we cannot find a similar result for the Al_2O_3/GaN interface. Usually, for various insulator/semiconductor interfaces, however, σ_n is assumed to be constant in the entire bandgap without an energy-dependent variation.[35–39] In particular, the exponential dependence of τ_{it} on energy in the GaN bandgap has been measured for the SiN/GaN interface and has been explained well by assuming that σ_n is constant in the bandgap.[35] According to previous reports, σ_n of 1×10^{-16} cm^2 can explain reasonably the properties of the Al_2O_3/GaN interface,[39] whereas σ_n of 2.4×10^{-17} cm^2 has been measured for the SiN/GaN

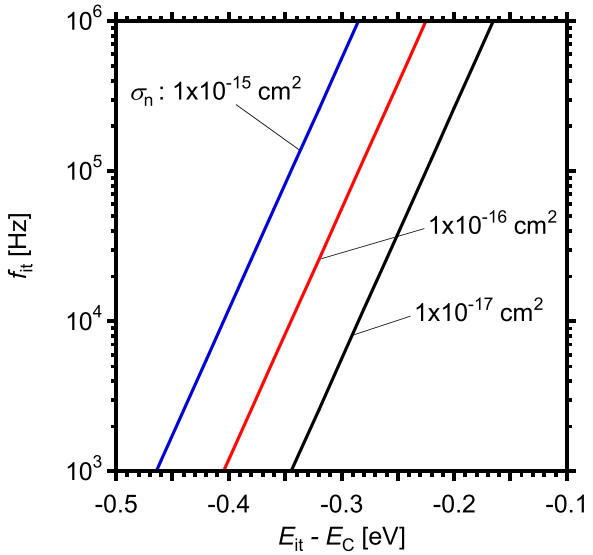

FIG. 6. Plot of $f_{it} = 1/\tau_{it}$ as a function of E_{it} for different σ_n values.

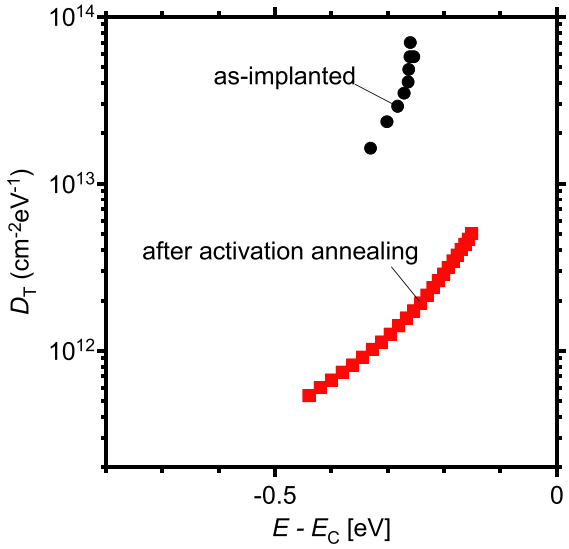

FIG. 7. D_{it} distributions at the ALD Al_2O_3/GaN interface formed with as-implanted GaN and that formed after activation annealing at 1250 °C. Data for the as-implanted sample are taken from our previous report. Taken with permission from Akazawa *et al.*, Jpn. J. Appl. Phys. **60**, 016502 (2021). Copyright 2020 The Japan Society of Applied Physics.

interface.[35] Therefore, assuming σ_n to be constant in the range of 10^{-15} to 10^{-17} cm^2 is appropriate. Considering the possible range of σ_n, the interface states between E_C − 0.15 and E_C − 0.45 eV can be derived from the C–V curves at measurement frequencies between 1 kHz and 1 MHz.

Regarding the 1 kHz and 1 MHz capacitances as C_{LF} and C_{HF}, respectively, we derived the D_{it} distribution in the range near E_C between E_C − 0.15 and E_C − 0.45 eV. The result is shown in Fig. 7 with the previously reported data[21] for the MOS diode formed with as-implanted GaN. Here, the density is denoted as D_T because the density of near-surface bulk defect states is included in the quoted data for the as-implanted sample. It can be seen that the discrete level around E_C − 0.25 eV observed for the as-implanted sample decreased by more than one order upon post-implantation annealing at 1250 °C, resulting in a continuous density distribution that is generally measured for interface states. The relatively low D_T in the range between E_C − 0.15 and E_C − 0.45 eV indicates that the damage caused by TMAH etching to remove the AlN cap layer was not severe. If the surface of Mg-implanted GaN after activation annealing is etched roughly with TMAH at near-surface defects, the interface disorder should have been severer, resulting in a higher D_T. On the contrary, there is a possibility that the TMAH treatment reduces D_T by smoothing the GaN surface or the interface, leading to the reduction in disorder at the interface. At a deeper point, D_T seems to be lower at least in the range of 10^{11} cm^{-2} eV^{-1}. Therefore, even a further reduction in D_T is possible by optimizing the fabrication process for the MOS structure.

According to the disorder-induced-gap-state model, the interface states originate from the disorder of the chemical bonds at the interface and the D_{it} distribution should be continuous and U-shaped in the entire bandgap.[40] However, a discrete level can be detected when the bulk defect level exists in the vicinity of the interface.[41,42] Since the concentration of the defects generated by implantation becomes maximum at the GaN surface even after annealing,[21–25] the defect levels might be detected by using MOS diodes. In the present results, however, only a continuous D_T distribution due to the interface disorder was detected near E_C, while no discrete levels due to near-surface defects were detected for the sample after activation annealing. This indicates that any defect levels did not affect the evaluation of D_T in the energy range from E_C − 0.15 to E_C − 0.45 eV. Therefore, we can conclude that the D_{it} distribution was obtained for the annealed sample. According to our previous report,[21] the discrete level at around E_C − 0.25 eV observed for the as-implanted sample shown in Fig. 7 was assigned to $V_N V_{Ga}$ defects. Therefore, the present results indicate that the $V_N V_{Ga}$ defects at the GaN surface were markedly reduced by activation annealing at 1250 °C. It has been reported that V_N and V_{Ga} agglomerate to form large complex defects upon annealing at a temperature similar to that in the present work, although $V_N V_{Ga}$ is the main defect species in the as-implanted GaN.[22–25] The residual near-surface bulk defect level seems to locate outside of this energy range, which might indicate that the agglomeration of defects changed the energy of defect level from E_C − 0.25 eV of $V_N V_{Ga}$ divacancies to outside the range between E_C − 0.15 and E_C − 0.45 eV.

The measured $N_D - N_A$ profile shown in Fig. 5(b) has been derived from the C–V curve in which the bias voltage was swept from the positive side to the negative side, within the range of the surface Fermi level located below E_C − 0.8 eV. The emission time constant of the interface states is given by the same formula as Eq. (3). Since the emission time constant of the interface states distributed below E_C − 0.8 eV should be much longer than 100 s with σ_n smaller than 10^{-15} cm^2, the response of the interface states cannot follow the DC bias change (50 mV/s). If the emission of electrons from the interface states and near-surface bulk defect levels

affects the C–V curve, the curve should have been stretched out and $N_D - N_A$ higher than that obtained within the detection range should have been derived. However, $N_D - N_A$ decreased at around the depth of 100 nm. This indicates that the effects of the interface states and near-surface bulk defect levels were negligible in the evaluation of the $N_D - N_A$ profile, and that the donors were compensated for. In Fig. 5(b), the measured $N_D - N_A$ profile deviates from the calculated profile assuming 100% activation of Mg acceptors. At the end of the implanted region, the deviation cannot be explained without assuming acceptor-like defects as described previously. There is a possibility that the origin of deviation is "the agglomeration of vacancy-type defects in the subsurface region" described in Ref. 23, although further studies are needed to confirm this.

On the other hand, V_N generates a defect level at $E_C - 0.07$ eV.[43] Since the detection range in this work is between $E_C - 0.15$ and $E_C - 0.45$ eV, the V_N defect level was outside the detection range. Therefore, there is a possibility that V_N remained even after annealing as reported previously.[16,22,23,29] The present results do not contradict the previous reports,[16,22,23,29] suggesting that the GL is caused by V_N-related defects.

IV. SUMMARY

The D_{it} distribution near E_C at the interface between ALD Al_2O_3 and Mg-ion-implanted GaN formed after activation annealing using the AlN cap layer and the subsequent cap layer removal has been measured. Mg ions were implanted lightly into n-GaN with the n-type conduction in GaN maintained even after the activation of Mg acceptors. Activation annealing was carried out at 1250 °C for 1 min using a 200-nm-thick AlN cap layer. XPS showed that the AlN cap layer was completely removed by wet etching using TMAH at 80 °C for 2 h. After annealing, the PL spectrum showed DAP emission with phonon coupling, which indicated the recovery from the implantation damage. The C–V characteristics of the completed MOS diode exhibited a non-negligible frequency dispersion. By applying the high–low-frequency capacitance method to the measured 1 kHz and 1 MHz C–V characteristics, we derived a continuous distribution of D_{it} monotonically increasing toward E_C in the range from $E_C - 0.15$ to $E_C - 0.45$ eV. Compared with the D_{it} distribution of the as-implanted sample, the density of the discrete level at $E_C - 0.25$ eV generated by $V_N V_{Ga}$ markedly decreased upon 1250 °C annealing.

ACKNOWLEDGMENTS

The authors thank Dr. T. Narita of Toyota Central R & D Labs., Inc., for the MOVPE growth of GaN epitaxial layers. This work was supported by the MEXT programs "Research and development of next-generation semiconductor to realize energy-saving society" (Grant No. JPJ005357) and "Creation of innovative core technology for power electronics" (Grant No. JPJ009777).

AUTHOR DECLARATIONS

Conflict of Interest

The authors have no conflicts to disclose.

Author Contributions

Yuki Hatakeyama: Conceptualization (equal); Data curation (equal); Investigation (lead). **Masamichi Akazawa**: Conceptualization (lead); Data curation (lead); Investigation (equal); Methodology (lead); Supervision (lead).

DATA AVAILABILITY

The data that support the findings of this study are available from the corresponding author upon reasonable request.

REFERENCES

[1] D. Ueda, in *Power GaN Devices*, edited by M. Meneghini, G. Meneghesso, and E. Zanoni (Springer, New York, 2017), Chap. 1.
[2] B. J. Baliga, Semicond. Sci. Technol. **28**, 074011 (2013).
[3] F. Schwierz, Solid-State Electron. **49**, 889 (2005).
[4] S. Kaneki, J. Ohira, S. Toiya, Z. Yatabe, J. T. Asubar, and T. Hashizume, Appl. Phys. Lett. **109**, 162104 (2016).
[5] T. Hashizume, S. Kaneki, T. Oyobiki, Y. Ando, S. Sasaki, and K. Nishiguchi, Appl. Phys. Express **11**, 124102 (2018).
[6] T. Yamada, D. Terashima, M. Nozaki, H. Yamada, T. Takahashi, M. Shimizu, A. Yoshigoe, T. Hosoi, T. Shimura, and H. Watanabe, Jpn. J. Appl. Phys. **58**, SCCD06 (2019).
[7] T. Nabatame, E. Maeda, M. Inoue, K. Yuge, M. Hirose, K. Shiozaki, N. Ikeda, T. Ohishi, and A. Ohi, Appl. Phys. Express **12**, 011009 (2019).
[8] B. N. Feigelson, T. J. Anderson, M. Abraham, J. A. Freitas, J. K. Hite, C. R. Eddy, and F. J. Kub, J. Cryst. Growth **350**, 21 (2012).
[9] T. J. Anderson, B. N. Feigelson, F. J. Kub, M. J. Tadjer, K. D. Hobart, M. A. Mastro, J. K. Hite, and C. R. Eddy, Electron. Lett. **50**, 197 (2014).
[10] J. D. Greenlee, T. J. Anderson, B. N. Feigelson, K. D. Hobart, and F. J. Kub, Phys. Status Solidi A **212**, 2772 (2015).
[11] T. J. Anderson, J. D. Greenlee, B. N. Feigelson, J. K. Hite, K. D. Hobart, and F. J. Kub, IEEE Trans. Semicond. Manuf. **29**, 343 (2016).
[12] K. Nomoto, K. Takahashi, O. Takuya, H. Ogawa, T. Nishimura, T. Mishima, H. G. Xing, and T. Nakamura, ECS Trans. **69**, 105 (2015).
[13] T. Oikawa, Y. Saijo, S. Kato, T. Mishima, and T. Nakamura, Nucl. Instrum. Methods Phys. Res., Sect. B **365**, 168 (2015).
[14] T. Narita, T. Kachi, K. Kataoka, and T. Uesugi, Appl. Phys. Express **10**, 016501 (2017).
[15] T. Niwa, T. Fujii, and T. Oka, Appl. Phys. Express **10**, 091002 (2017).
[16] H. Sakurai, M. Omori, S. Yamada, Y. Furukawa, H. Suzuki, T. Narita, K. Kataoka, M. Horita, M. Bockowski, J. Suda, and T. Kachi, Appl. Phys. Lett. **115**, 142104 (2019).
[17] G. Alfieri, V. K. Sundaramoorthy, and R. Micheletto, J. Appl. Phys. **123**, 205303 (2018).
[18] M. Akazawa, N. Yokota, and K. Uetake, AIP Adv. **8**, 025310 (2018).
[19] M. Akazawa and K. Uetake, Jpn. J. Appl. Phys. **58**, SCCB10 (2019).
[20] M. Akazawa, R. Kamoshida, S. Murai, T. Narita, M. Omori, J. Suda, and T. Kachi, Phys. Status Solidi B **257**, 1900367 (2020).
[21] M. Akazawa, R. Kamoshida, S. Murai, T. Kachi, and A. Uedono, Jpn. J. Appl. Phys. **60**, 016502 (2021).
[22] A. Uedono, S. Takashima, M. Edo, K. Ueno, H. Matsuyama, H. Kudo, H. Naramoto, and S. Ishibashi, Phys. Status Solidi B **252**, 2794 (2015).
[23] A. Uedono, S. Takashima, M. Edo, K. Ueno, H. Matsuyama, W. Egger, T. Koschine, C. Hugenschmidt, M. Dickmann, K. Kojima, S. F. Chichibu, and S. Ishibashi, Phys. Status Solidi B **255**, 1700521 (2018).
[24] H. Iguchi, T. Narita, K. Kataoka, M. Kanechika, and A. Uedono, J. Appl. Phys. **126**, 125102 (2019).

[25]A. Uedono, H. Iguchi, T. Narita, K. Kataoka, W. Egger, T. Koschine, C. Hugenschmidt, M. Dickmann, K. Shima, K. Kojima, S. F. Chichibu, and S. Ishibashi, Phys. Status Solidi B **256**, 1900104 (2019).
[26]M. Kodama, M. Sugimoto, E. Hayashi, N. Soejima, O. Ishiguro, M. Kanechika, K. Itoh, H. Ueda, T. Uesugi, and T. Kachi, Appl. Phys. Express **1**, 021104 (2008).
[27]H. G. Grimmeiss and B. Monemar, J. Appl. Phys. **41**, 4054 (1970).
[28]R. Dingle and M. Ilegems, Solid State Commun. **9**, 175 (1971).
[29]K. Kojima, S. Takashima, M. Edo, K. Ueno, M. Shimizu, T. Takahashi, S. Ishibashi, A. Uedono, and S. F. Chichibu, Appl. Phys. Express **10**, 061002 (2017).
[30]K. Shima, H. Iguchi, T. Narita, K. Kataoka, K. Kojima, A. Uedono, and S. F. Chichibu, Appl. Phys. Lett. **113**, 191901 (2018).
[31]S. M. Sze and K. K. Ng, *Physics of Semiconductor Devices*, 3rd ed. (Wiley, Hoboken, NJ, 2007), Chap. 4.
[32]W. Shockley and W. T. Read, Phys. Rev. **87**, 835 (1952).
[33]P. Hacke, T. Detchprohm, K. Hiramatsu, N. Sawaki, K. Tadatomo, and K. Miyake, J. Appl. Phys. **76**, 304 (1994).
[34]E. H. Nicollian and J. R. Brews, *MOS (Metal Oxide Semiconductor) Physics and Technology* (Wiley, Hoboken, NJ, 2003), Chap. 7.
[35]B. Gaffey, L. J. Guido, X. W. Wang, and T. P. Ma, IEEE Trans. Electron Devices **48**, 458 (2001).
[36]G. Brammertz, K. Martens, S. Sioncke, A. Delabie, M. Caymax, M. Meuris, and M. Heyns, Appl. Phys. Lett. **91**, 133510 (2007).
[37]G. Brammertz, H. C. Lin, K. Martens, D. Mercier, C. Merckling, J. Penaud, C. Adelmann, S. Sioncke, W. E. Wang, M. Caymax, M. Meuris, and M. Heyns, J. Electrochem. Soc. **155**, H945 (2008).
[38]M. Matys, R. Stoklas, J. Kuzmik, B. Adamowicz, Z. Yatabe, and T. Hashizume, J. Appl. Phys. **119**, 205304 (2016).
[39]K. Nishiguchi, K. Nakata, and T. Hashizume, J. Appl. Phys. **132**, 175302 (2022).
[40]H. Hasegawa and H. Ohno, J. Vac. Sci. Technol. B **4**, 1130 (1986).
[41]T. Sawada, K. Numata, S. Tohdoh, T. Saitoh, and H. Hasegawa, Jpn. J. Appl. Phys. **32**, 511 (1993).
[42]T. Hashizume and R. Nakasaki, Appl. Phys. Lett. **80**, 4564 (2002).
[43]Z.-Q. Fang, D. C. Look, W. Kim, Z. Fan, A. Botchkarev, and H. Morkoç, Appl. Phys. Lett. **72**, 2277 (1998).